Hybrid Estimator-Based Harmonic Robust Grid Synchronization Technique

Ahmed, H., Pay, M. L., Benbouzid, M., Amirat, Y. & Elbouchikhi, E.

Original citation & hyperlink:
Ahmed, H, Pay, ML, Benbouzid, M, Amirat, Y & Elbouchikhi, E 2019, 'Hybrid Estimator-Based Harmonic Robust Grid Synchronization Technique' Electric Power Systems Research, vol. 177, 106013.
https://dx.doi.org/10.1016/j.epsr.2019.106013

DOI 10.1016/j.epsr.2019.106013
ISSN 0378-7796

Publisher: Elsevier

Hybrid Estimator-Based Harmonic Robust Grid Synchronization Technique

Hafiz Ahmed[a,*], Miao Lin Pay[b], Mohamed Benbouzid[c,e], Yassine Amirat[d], Elhoussin Elbouchikhi[d]

[a]*School of Mechanical, Aerospace and Automotive Engineering, Coventry University, Coventry CV1 5FB, United Kingdom*
[b]*School of Engineering and Technology, University of Hertfordshire, Hatfield, Hertfordshire, AL10 9AB, United Kingdom*
[c]*University of Brest, UMR CNRS 6027 IRDL, 29238 Brest, France*
[d]*ISEN Brest, Yncréa Ouest, UMR CNRS 6027 IRDL, 29200 Brest, France*
[e]*Shanghai Maritime University, 201306 Shanghai, China*

Abstract

Harmonic robust grid synchronization technique has been studied in this paper. This implies the estimation of phase and frequency of single-phase grid voltage signal. Motivated by recent developments in linear harmonic oscillator based technique, this paper first propose an adaptive observer based solution that has the potential to speed-up the dynamic performance with respect to other generalized integrator type techniques. However, this may decrease the robustness of the proposed technique in the presence of harmonics and or DC bias. To overcome this issue, a hybrid estimator is proposed. This estimator is comprised of a band-pass type pre-loop filter and the initially proposed adaptive observer. Local stability and tuning of the adaptive observer are provided for the nominal case. In the presence of harmonics, small-signal modeling and tuning of the hybrid estimator are provided as well. Finally, hardware-in-the-loop (HIL) comparative experimental results are provided with similar other recently proposed techniques in the literature. Experimental results demonstrate the suitability of the proposed techniques.

Keywords: Frequency Estimation, Grid Synchronization, Phase Estimation, Prefiltering, Harmonic Robust Estimation

1. Introduction

Climate change is a serious concerns of current time. Use of renewable energy sources have been identified as a potential solution to tackle the climate change issue by reducing the carbon footprint. This has led to the revolution in the grid integration of renewable energy sources. Renewable energy sources are generally connected to the existing power network through grid-tied converters. As a result, control and synchronization of grid-tied converters has attracted lot of attention in recent time.

There are various types of grid synchronization techniques available in the literature. Out of which synchronizing current controller is undoubtedly the most popular one. This kind of controllers require the precise and fast estimation of grid signal parameters. In addition to this, many other applications also require the various grid signal parameters. This led to the extensive research in estimating the parameters of grid voltage signal.

There are several widely accepted class of techniques available in the literature. Some of the popular techniques are: discrete Fourier transform (DFT) [1], regression based techniques (recursive least-square, weighted least-square etc.) [2–4], open-loop techniques [5], statistical approaches [6–8], state-space filtering (Kalman filter and various variants) [9], artificial neural networks [10], phase-locked loop (PLL) [11–24], global adaptive observers [25], nonlinear filtering techniques: second-order generalized integrator - frequency-locked loop (SOGI-FLL) [26, 27], enhanced phase-locked loop (EPLL) [28], limit cycle oscillator [29, 30], adaptive notch filter [31, 32], discrete adaptive filter [33], etc.

Out of various techniques mentioned in the previous paragraph, PLL type techniques are undoubtedly the most popular ones in the research literature and also in the industrial applications. PLL is a feedback system that uses the power of feedback to achieve the locking of the PLL system w.r.t. the input signal. PLL in general performs satisfactorily, however the performance degrades in the presence of harmonics and or disturbances. Moreover, there is trade-off between convergence speed and disturbance rejection capabilities. To overcome the limitations of standard PLL type technique, several nonlinear techniques (including various variations of PLL) have been proposed. EPLL is one of them. SOGI-FLL and its nonlinear variants [29, 30, 34], use frequency adaptive harmonic oscillator as quadrature signal generator (QSG). SOGI-FLL and its nonlinear variants are harmonic robust and provides good balance between disturbance rejection and convergence speed. As such, the linear QSG model used by SOGI type techniques are considered for further development in this work.

Due to the structure of the SOGI-FLL, arbitrary complex conjugate pole placement is not possible (*cf.* Sec-2.1). As such limited dynamic tuning is possible which may re-

*Corresponding author
Email address: `hafiz.h.ahmed@ieee.org` (Hafiz Ahmed)

sult in slower transient performance. To overcome this limitation, in this paper, we first propose a modification that allows arbitrary complex conjugate pole placement. The proposed modification allows to make the dynamic response faster. However, fast dynamic response comes at the cost of robustness reduction in the presence of harmonics. There are two popular types of solution available in the literature to enhance the harmonic robustness for SOGI-FLL type techniques. In the first category, multiple parallel SOGI filters together with one FLL block are proposed in the literature [27]. This technique can provide very good performance with zero steady-state error. However, this is only possible in the case of known harmonic components. If the harmonic components are not known completely, then by using a large number of filters (with *a priori* knowledge of the grid), acceptable performance can be guaranteed. In any case, this technique is computationally demanding.

In the second category, harmonic robustness is added by using a SOGI-type frequency adaptive pre-loop filter which works as a band-pass filter [35–37]. The advantage of this approach is that it can provide harmonic robustness without much additional computational complexity. This feature can be very useful for low-cost micro-controllers based control system design where computational complexity is of serious concern. Moreover, this approach also helps to eliminate the DC bias. That is why, in this paper, we focus on using pre-loop filtering to enhance the harmonic robustness of the adaptive observer. The resulting hybrid estimator eliminates the effect of DC bias and provide better robustness to harmonics.

The rest of the paper is organized as follows: Sec. 2 describes the development of the proposed estimator in the nominal case. Development of the hybrid estimator to tackle the effect of harmonics and or DC bias is given in Sec. 3. Experimental results are given in Sec. 4 while Sec. 5 concludes this paper.

2. Development of Estimator: Nominal Case

2.1. Background and Motivation

A single-phase grid voltage signal is given by:

$$y(t) = A\sin\underbrace{(\omega t + \phi)}_{\theta} \tag{1}$$

where A is the amplitude, ϕ is the phase, $\omega = 2\pi f$ is the frequency and $\theta \in [0, 2\pi)$ is the instantaneous phase. The in-quadrature signal of $y(t)$ is given by $x(t) = -A\cos(\theta)$. Then by considering $\xi = [x(t)\; y(t)]^T$ as the state vector, the grid voltage dynamics can be written as:

$$\dot{\zeta} = \begin{bmatrix} 0 & \omega \\ -\omega & 0 \end{bmatrix} \zeta = \bar{A}\zeta \tag{2}$$

$$y = \begin{bmatrix} 0 & 1 \end{bmatrix} \zeta = \bar{C}\zeta \tag{3}$$

The grid dynamics is observable. If the grid frequency ω is known, then estimating the states of grid dynamics from the available measurement y are straightforward. However, in practice the grid frequency may not be known precisely and can be time-varying. Frequency-locked loop can be very useful to estimate the unknown frequency. SOGI-FLL is one of the most popular frequency locked-loop available in the literature that uses the model (2)-(3) to generate the quadrature signals. In the observer-based notation, SOGI-FLL with gain normalization can be written as [27]:

$$\dot{\hat{\zeta}} = \hat{\bar{A}}\hat{\zeta} + \bar{L}(y - \bar{C}\hat{\zeta}) \tag{4}$$

$$\dot{\hat{\omega}} = \dot{z} = \frac{-\Gamma(y - C\hat{\zeta})\hat{x}k\hat{\omega}}{\hat{x}^2 + \hat{y}^2} \tag{5}$$

where, the estimated values are indicated by $\hat{}$, $\hat{\omega} = \omega_n + z$ is the estimated unknown frequency, $\bar{L} = \begin{bmatrix} 0 & k\hat{\omega} \end{bmatrix}$ and $k, \Gamma > 0$ are the tuning parameters. In the steady-state, *i.e.* $\omega = \hat{\omega}$, the observer error dynamics is represented by the matrix $\bar{A} - \bar{L}\bar{C}$. The eigenvalues of the error dynamics are $-\frac{k\omega}{2} \pm \omega\sqrt{k^2 - 4}$. Since the system is of oscillating nature, complex conjugate poles are always desired. However, for any $k \geq 2$, the closed loop system eigenvalues only have real parts. Moreover, for $0 < k < 2$, the range of the real part of the closed-loop pole location are always less than $-\omega$. Since the settling time is determined by the closed-loop pole location, the transient response can be slow. This motivates the proposed work to address the potential slow-transient response of SOGI-FLL. The following section describes the proposed development.

2.2. SOGI-QSG type adaptive observer design

One idea to make the transient response faster is to use coordinate transformation [25]. This may speed up the convergence speed. To this end, let us consider the following coordinate transformation:

$$\eta = \frac{1}{2\omega} \begin{bmatrix} 1 & 1 \\ -1 & 1 \end{bmatrix} \zeta = T\zeta \tag{6}$$

In the transformed coordinate, system (2)-(3) can be written as:

$$\dot{\eta} = A\eta \tag{7}$$

$$y = C\eta \tag{8}$$

where $A = T\bar{A}T^{-1} = \bar{A}$ and $C = \bar{C}T^{-1} = [\omega \quad \omega]$. Then the following linear observer can be proposed for system (7)-(8):

$$\dot{\hat{\eta}} = \hat{A}\hat{\eta} + L(y - \hat{C}\hat{\eta}) \tag{9}$$

$$\hat{y} = \hat{C}\hat{\eta} \tag{10}$$

where $L = [l_1 \; l_2]^T$ is the observer gain matrix to be tuned and $\hat{}$ represents estimated value. In the nominal case *i.e.* $\omega = \hat{\omega} = \omega_n$, the two in-quadrature output signals of the adaptive observer is given by:

$$D(s) = \frac{\hat{y}(s)}{y(s)} = \frac{(l_1 + l_2)\hat{\omega}s + (l_2 - l_1)\hat{\omega}^2}{s^2 + (l_1 + l_2)\hat{\omega}s + (l_2 - l_1 + 1)\hat{\omega}^2} \tag{11}$$

$$Q(s) = \frac{\hat{x}(s)}{y(s)} = \frac{(l_1 - l_2)\hat{\omega}s + (l_2 + l_1)\hat{\omega}^2}{s^2 + (l_1 + l_2)\hat{\omega}s + (l_2 - l_1 + 1)\hat{\omega}^2} \tag{12}$$

If the observer gains are chosen as $l_1 = l_2 = l$, which corresponds to closed-loop observer poles in $-l\omega + \omega\sqrt{(l-1)(l+1)}$, then the transfer functions of SOGI-FLL (Eq. (2) in [27]) can be recovered from Eq. (11)-(12). As such the adaptive observer and SOGI-QSG are dynamically equivalent in the frequency domain subject to parameter tuning. Bode diagrams of the transfer functions given by eq. (11) and (12) are given in Fig. 1. Bode diagram are given here to show the frequency domain characteristics of the proposed adaptive observer.

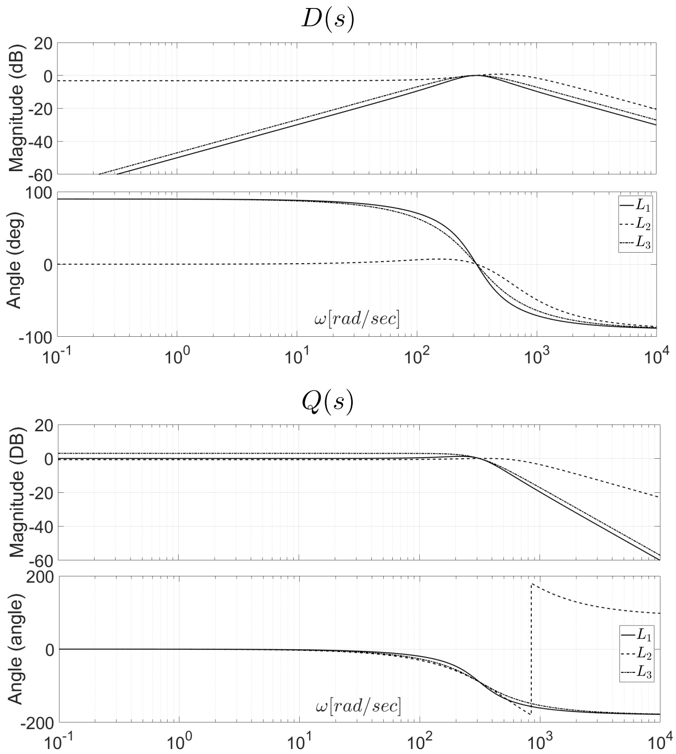

Figure 1: Bode diagrams of the transfer functions (11) and (12) for different observer gains. Transfer functions are obtained by considering closed-loop poles in $-\omega_n/2 \pm i\sqrt{3}\omega_n/2$, $-1.5\omega_n \pm i\omega_n$ and $\omega_n/\sqrt{2} \pm i\sqrt{\omega_n}/2$ corresponding to $L_1 = [0.5; 0.5]$, $L_2 = [0.375; 2.6250]$ and $L_3 = [1/\sqrt{2}; 1/\sqrt{2}]$ respectively.

From the estimated states in $\hat{\eta}$-coordinate, the original state variables can be obtained by the following relationship:

$$\hat{\zeta} = \hat{\omega} \begin{bmatrix} 1 & -1 \\ 1 & 1 \end{bmatrix} \hat{\eta} = \hat{T}^{-1}\hat{\eta} \tag{13}$$

Using the estimated $\hat{\zeta}$, the instantaneous phase can be calculated as:

$$\hat{\theta} = \arctan\{\hat{y}/(-\hat{x})\} \tag{14}$$

FLL design

Observer (9)-(10) requires the estimated value of the frequency $\hat{\omega}$. FLL can be very suitable for this purpose. Following the ideas presented in [27], a similar FLL can also be adopted in this case. The adopted FLL is given by:

$$\dot{\hat{\omega}} = \dot{\hat{z}} = -\mu\hat{\omega}(y - \hat{C}\hat{\eta})\hat{\eta}_1 \tag{15}$$

where $\mu > 0$ is the tuning parameter and $(y - \hat{C}\hat{\eta})$ is the output estimation error. To understand the idea behind the proposed FLL, let us consider the transfer functions of the FLL variables for the nominal frequency case given below:

$$\frac{\eta_1}{y}(s) = \frac{l_1 s + l_2\omega_n}{s^2 + s(l_1 + l_2)\omega_n + (l_2 - l_1 + 1)\omega_n^2} \tag{16}$$

$$\frac{E}{y}(s) = \frac{s^2 + \omega_n^2}{s^2 + s(l_1 + l_2)\omega_n + (l_2 - l_1 + 1)\omega_n^2} \tag{17}$$

where $E = y - C\eta$. The angle plot of the bode diagrams of the FLL variables with $l_1 = 0.3750$ and $l_2 = 2.6250$ (corresponds to closed-loop poles in $-1.5\omega_n \pm i\omega_n$) are given in Fig. 2.

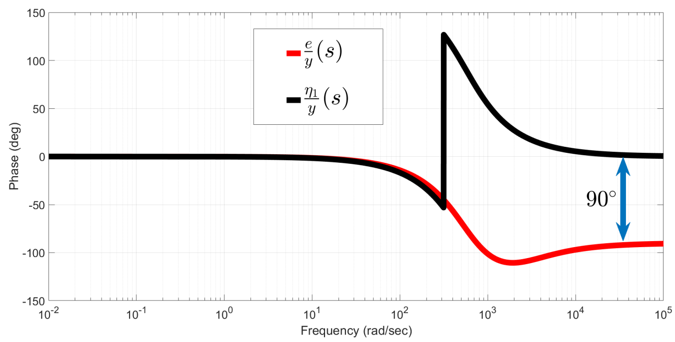

Figure 2: Angle plot of the input variables of the proposed FLL.

It can be seen from Fig. 2 that FLL input variables have angle difference of $\approx 0^\circ$ near ω_n. However, the angle difference is $\approx 90^\circ$ when $\omega > \omega_n$. This idea is similar to the idea of FLL, given in Fig. 4 of [27]. FLL (15) doesn't use any gain normalization. This may introduce large errors when the grid voltage amplitude suffers from huge jumps. To avoid this problem, using ideas similar to [27], the following gain normalized FLL is going to be considered in this work:

$$\dot{\hat{\omega}} = \dot{\hat{z}} = -\frac{\mu\hat{\omega}(y - \hat{C}\hat{\eta})\hat{\eta}_1 l}{\hat{\eta_1}^2 + \hat{\eta_2}^2} \tag{18}$$

where $l = \sum_{i=1}^{2} l_i$.

2.3. Stability analysis and tuning

For further analysis, we name the proposed method as adaptive observer - FLL (AO-FLL). To analyze the stability of the AO-FLL, let us consider the observer dynamics in the original ζ coordinate. In the ζ coordinate, estimated state variables can be written as $\hat{x}(t)$ and $\hat{y}(t)$. The the observer (9)-(10) and FLL dynamics (18) in terms of state variables $\hat{x}(t)$ and $\hat{y}(t)$ are given as:

$$\dot{\hat{x}} = \hat{\omega}\hat{y} + (l_1 - l_2)\hat{\omega}(y - \hat{y}) \tag{19}$$

$$\dot{\hat{y}} = -\hat{\omega}\hat{x} + (l_1 + l_2)\hat{\omega}(y - \hat{y}) \tag{20}$$

$$\dot{\hat{\omega}} = -(\mu l \hat{\omega}^2/(\hat{x}^2 + \hat{y}^2))(y - \hat{y})(\hat{x} + \hat{y}) \tag{21}$$

Then the dynamics of the observer in polar coordinate (r, θ) [38] are given as:

$$\dot{r} = \hat{\omega}e\{(l_2 - l_1)\cos(\theta - \Delta\theta) + (l_1 + l_2)\sin(\theta - \Delta\theta)\} \tag{22}$$

$$\dot{\Delta\theta} = -\omega + \hat{\omega} - r^{-1}e\hat{\omega}(l_1 + l_2)\cos(\theta - \Delta\theta) + r^{-1}e\hat{\omega}(l_1 - l_2)\sin(\theta - \Delta\theta) \tag{23}$$

$$\dot{\hat{z}} = -\mu l \hat{\omega}^2 r^{-1} e\{\sin(\theta - \Delta\theta) + \cos(\theta - \Delta\theta)\} \tag{24}$$

where $\Delta\theta = \theta - \hat{\theta}$, $e = A\sin(\theta) - r\sin(\theta - \Delta\theta)$. Through the phase error $\Delta\theta$, the AO-FLL is coupled with the actual grid voltage dynamics. As a result, stability of the AO-FLL dynamics in polar coordinate (19)-(21) implies the convergence (*i.e.* $\eta - \hat{\eta} \to 0$) of the observer. The desired equilibrium of Eq. (19)-(21) is given as:

$$x^\star = \{r = A, \Delta\theta = 0, z = \omega - \omega_n\} \tag{25}$$

The Jacobian matrix of the AO-FLL dynamics in polar coordinates (19)-(21) evaluated at $x^\star$ is given at the bottom of this page. The eigenvalues $J(x^\star)$ can be calculated from the characteristic equation given by:

$$\begin{gathered}\det(sI_3 - J(x^\star)) = 0 \\ s^3 + \omega_n(l_1 + l_2)s^2 + \\ \frac{1}{2}[l\mu\omega_n^2\{\sqrt{2}\sin(2\theta + \pi/4) + 1\}]s = 0\end{gathered} \tag{26}$$

The roots of the polynomial (26) are 0, $-\omega_n l/2 \pm (1/2)\sqrt{\kappa}$ where $\kappa = l^2 - 4l\mu\cos^2(\theta) - l\mu 2\sin(2\theta)$. Since $-1 \leq \sin(2\theta) \leq 1$ and $0 \leq \cos^2(\theta) \leq 1$, then for properly selected values of l and μ, it can be guaranteed that $l^2 - 4l\mu\cos^2(\theta) - l\mu 2\sin(2\theta) < \omega_n^2$. This implies that real-part of the eigenvalues of $J(x^\star)$ are always ≤ 0 which concludes the marginal stability of AO-FLL.

Gain tuning

Observer gain matrix L and frequency identification parameter μ characterizes the response of AO-FLL. Gain matrix L can be tuned using standard pole placement approach. Let us select the desired closed-loop poles as $-1.5\omega_n \pm i\omega_n$. Then using the `place` command in Matlab, $L = [0.375 \ 2.6250]^T$ is found as the gain matrix. As a result, $l = \sum_{i=1}^{2} l_i = 3$. The parameter μ determines the convergence speed of the frequency estimation. High value of μ increases the convergence speed, peak overshoot, *etc.* and vice-versa. As such μ has to be selected as a trade-off between fast dynamic response vs. peak overshoot. Through extensive simulation study we found $\mu = 0.05$ as a good value.

To implement the proposed technique, Eq. (9),(10), (14) and (18) are required. Block diagram of the proposed approach is given in Fig. 3.

3. Development of Hybrid Estimator

As mentioned in the Introduction, faster dynamic response of AO-FLL comes at the cost of reduction in robustness to harmonics. To overcome this problem, frequency adaptive pre-filtering can be considered. Based on the idea presented in [37], an hybrid estimator named as AO-FLL with pre-loop filter (AO-FLL-WPF) is proposed in this work and given in Fig. 4. As seen from Fig. 4, AO-FLL-WPF has one more parameters to tune than that of AO-FLL. To minimize the number of parameters to tune, the gain-normalized FLL ((18)) can be re-written as:

$$\dot{\hat{\omega}} = \dot{z} = \frac{-l\hat{\omega}^3(y - \hat{C}\hat{\eta})\hat{\eta}_1}{(2\hat{\omega}\hat{\eta}_1)^2 + (2\hat{\omega}\hat{\eta}_2)^2} \tag{27}$$

This eliminates the tuning of the parameter μ. As a result, total number parameters to tune for both techniques remain the same. To analyze the stability and tuning of AO-FLL-WPF, small-signal modeling can be very useful. For this purpose, first the small-signal modeling of AO-FLL can be done. Then by cascading the pre-filter, the small signal model of the hybrid estimator can easily be obtained

3.1. Small-Signal Modeling of AO-FLL

By substituting the value of ζ in Eq. (6), the the dynamics of AO-FLL can be studied in the $\eta-$coordinate. In the $\eta-$coordinate, FLL dynamics (27) can be written as:

$$J(x^\star) = \begin{bmatrix} -\hat{\omega}\sin(\theta)\{(l_1 + l_2)\sin(\theta) + (l_1 - l_2)\cos(\theta)\} & r\hat{\omega}\cos(\theta)\{(l_1 + l_2)\sin(\theta) + (l_1 - l_2)\cos(\theta)\} & 0 \\ -\frac{1}{2r}\hat{\omega}(l_1 + l_2)\sin(2\theta) - \frac{1}{r}\hat{\omega}\sin^2(\theta)(l_1 - l_2) & \frac{1}{2}\hat{\omega}(l_1 - l_2)\sin(2\theta) - \hat{\omega}\cos^2(\theta)(l_1 + l_2) & 1 \\ l\mu r^{-1}\hat{\omega}^2\sin(\theta)\{\cos(\theta + \sin(\theta))\} & -l\mu\hat{\omega}^2\cos(\theta)\{\cos(\theta + \sin(\theta))\} & 0 \end{bmatrix}$$

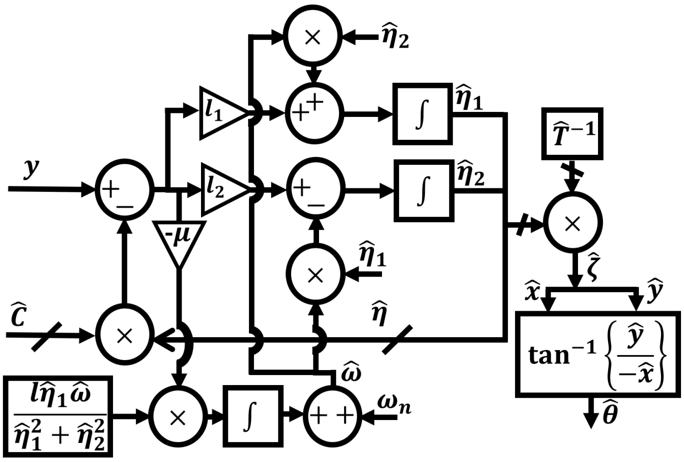

Figure 3: Block diagram of the AO-FLL where matrix multiplication is indicated by $\nrightarrow$.

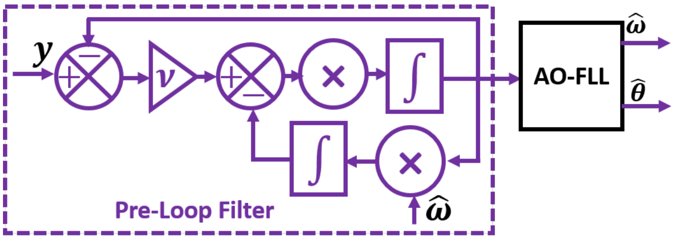

Figure 4: Block Diagram of AO-FLL-WPF.

$$
\begin{aligned}
\dot{\hat{\omega}} &= \frac{l\hat{\omega}^3}{2\hat{\omega}\hat{A}^2}\{A\sin(\theta) - \hat{A}\sin(\hat{\theta})\}\{\hat{A}\cos(\hat{\theta}) - \hat{A}\sin(\hat{\theta})\} \\
&= (l/2)\hat{\omega}^2\hat{A}^{-1}\{A\sin(\theta) - \hat{A}\sin(\hat{\theta})\}\{\cos(\hat{\theta}) - \sin(\hat{\theta})\}
\end{aligned} \tag{28}
$$

The last term in Eq. (28) is always bounded since

$$
\begin{aligned}
\cos(\hat{\theta}) - \sin(\hat{\theta}) &= \sqrt{2}\{\cos(\hat{\theta})\cos(\pi/4) - \sin(\hat{\theta})\sin(\pi/4)\} \\
&= \sqrt{2}\cos(\hat{\theta} - \pi/4)
\end{aligned}
$$

Moreover, the maximum value of $|\cos(\hat{\theta}) - \sin(\hat{\theta})|$ is $\sqrt{2}$ since $-1 \leq \cos(\hat{\theta}-\pi/4) \leq 1$. Then by applying small-angle approximation formula i.e. $\sin(\theta) \approx \theta$ and also assuming quasi-locked condition with $A \approx \hat{A}$ and $\hat{\omega} = \omega_n$, the FLL dynamics (28) in linear form can be written as:

$$
\dot{\hat{\omega}} = (l/2)\omega_n^2\left(\theta - \hat{\theta}\right) \tag{29}
$$

The phase dynamics can be obtained from Eq. (14) as follows:

$$
\begin{aligned}
\dot{\hat{\theta}} &= \frac{\dot{\hat{x}}\hat{y} + \dot{\hat{y}}\hat{x}}{\hat{x}^2 + \hat{y}^2} \\
&= \frac{\hat{\omega}\hat{A}^2 - \hat{\omega}l\hat{x}_\alpha(y - \hat{y})}{\hat{A}^2}
\end{aligned} \tag{30}
$$

By using Eq. (28) into Eq. (30), the following can be obtained:

$$
\dot{\hat{\theta}} = \hat{\omega} + \dot{\hat{\omega}}\hat{\omega}^{-1} \tag{31}
$$

Model (31) is nonlinear due to the presence of nonlinear multiplication in the second term of the right-hand side. In order to apply the linear technique, let us assume that $\hat{\omega} = \omega_n$. Then Eq. (31) results in,

$$
\dot{\hat{\theta}} = \hat{\omega} + \dot{\hat{\omega}}\omega_n^{-1} \tag{32}
$$

Finally, the amplitude estimation dynamics can be written as:

$$
\begin{aligned}
\hat{A} &= \sqrt{\hat{x}^2 + \hat{y}^2} \\
\dot{\hat{A}} &= \frac{\hat{x}\dot{\hat{x}} + \hat{y}\dot{\hat{y}}}{\sqrt{\hat{y}^2 + \hat{x}^2}} \\
&= (l/2)\hat{\omega}\{2A\sin(\theta)\sin(\hat{\theta}) - 2A\sin(\theta)\cos(\hat{\theta})\} \\
&+ (l/2)\hat{\omega}\{-2\hat{A}\sin^2(\hat{\theta}) + \hat{A}\sin(2\hat{\theta})\}
\end{aligned} \tag{33}
$$

The right-hand side of Eq. (33) can be simplified as:

$$
\begin{aligned}
&2A\sin(\theta)\sin(\hat{\theta}) - 2A\sin(\theta)\cos(\hat{\theta}) - 2\hat{A}\sin^2(\hat{\theta}) + \hat{A}\sin(2\theta) \\
&= A\{\cos(\theta - \hat{\theta}) - \cos(\theta + \theta)\} - 2A\sin(\theta)\cos(\hat{\theta}) \\
&\hat{A}\sin(2\theta) - \hat{A}(1 - \cos(2\hat{\theta}))
\end{aligned} \tag{34}
$$

Then substituting Eq. (34) in (33) along with the quasi-locked condition assumption results in:

$$
\dot{\hat{A}} = (l/2)\omega_n\left(A - \hat{A}\right) \tag{35}
$$

In deriving Eq. (35), small-angle approximation formulas are used.

Eq. (29), (32) and (35) describes the linear model of the QSG-FLL. Based on these Equations, the linearized model of the AO-FLL is given in Fig. 5. From Fig. 5, following closed-loop transfer functions are obtained:

$$
\dot{\hat{A}} = \frac{l\omega_n/2}{s + l\omega_n/2}A(s) \tag{36}
$$

$$
\dot{\hat{\omega}} = \frac{l\omega_n^2/2}{s^2 + (l\omega_n/2)s + l\omega_n^2/2}\omega(s) \tag{37}
$$

$$
\dot{\hat{\theta}} = \frac{(l\omega_n/2)s + l\omega_n^2/2}{s^2 + (l\omega_n/2)s + l\omega_n^2/2}\theta(s) \tag{38}
$$

3.2. Small-Signal Modeling of AO-FLL-WPF

AO-FLL-WPF uses SOGI-type band-pass filter (S-BPF) with frequency feedback from AO-FLL to remove the harmonics and DC bias from the grid signal. Filtered signal is then fed to the AO-FLL. The block diagram of AO-FLL-WPF is given in Fig. 4. Since AO-FLL-WPF uses S-BPF,

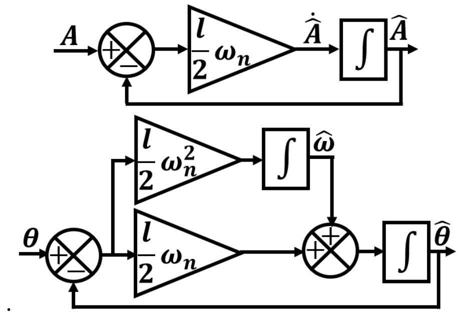

Figure 5: Linearized model of AO-FLL.

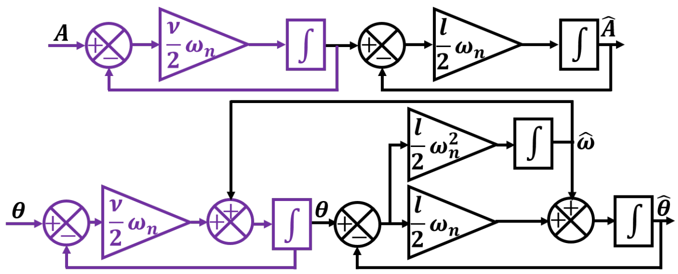

Figure 6: Linearized model of AO-FLL-WPF.

then by cascading SOGI-model with AO-FLL model, the linearized model of AO-FLL-WPF can be easily obtained and given in Fig. 6. The closed-loop transfer functions of the AO-FLL-WPF, obtained through Fig. 6 are given below:

$$\frac{\hat{A}(s)}{A(s)} = \frac{(l\omega_n/2)(\nu\omega_n/2)}{(s+(l\omega_n/2))(s+(\nu\omega_n/2))} \tag{39}$$

$$\frac{\hat{\omega}(s)}{\omega(s)} = \frac{\nu l\omega_n^3/4}{s^3+((\nu+l)\omega_n/2)s^2+(\nu l\omega_n^2/4)s+\nu l\omega_n^3/4} \tag{40}$$

$$\frac{\hat{\theta}(s)}{\theta(s)} = \frac{(\mu l\omega_n^2/4)s+\nu l\omega_n^3/2}{s^3+((\nu+l)\omega_n/2)s^2+(\nu l\omega_n^2/4)s+\nu l\omega_n^3/4} \tag{41}$$

AO-FLL-WPF has two parameters to tune i.e. S-BPF gain ν and the observer gain L. To tune the two gains, let us consider the closed-loop amplitude estimation transfer function (39). The denominator polynomial is given by:

$$s^2 + \underbrace{(\frac{l\omega_n}{2}+\frac{\nu\omega_n}{2})}_{2\zeta\omega'} s + \underbrace{\frac{l\nu\omega_n^2}{4}}_{\omega'^2} = 0 \tag{42}$$

Let us assume that $l=\nu$ and $\omega'=\omega_n$. Then for the optimal damping ratio of $\zeta = 1/\sqrt{2}$ (often suggested in the literature for second-order system), the gains can be found as $l=\nu=1/\sqrt{2}$. For $\nu = 1/\sqrt{2}$, the closed-loop poles of the S-BPF are $\omega_n\,(0.35 \pm 0.93i)$. If we chose the same closed-loop poles for the AO part, then by applying `place` command in Matlab, the observer gain is found to be $L = [1/2\sqrt{2} \quad 1/2\sqrt{2}]^T$. With the selected ν and l, all the closed-loop transfer functions i.e. Eq. (36)-(41) are stable. While tuning AO-FLL-WPF, readers should be careful of the pre-loop filter's bandwidth. Pre-loop filter depends on the estimated frequency obtained from the adaptive observer block. As such, the bandwidth of the pre-loop filter determines the bandwidth of the whole system. As a general rule of thumb, pre-loop filter's closed loop poles shouldn't be higher than that of the adaptive observer.

4. Results and Discussions

To evaluate the performance of the AO-FLL, dSPACE 1104 board based hardware-in-the-loop (HIL) experimental studies are considered.

4.1. Without pre-filter

This Section describe the experimental results for AO-FLL. As comparison technique, we have selected SOGI-FLL [27]. The parameters of these techniques are selected as, SOGI-FLL [27]: $k=\sqrt{2}$, $\Gamma=50$, AO-FLL: $L=[0.375\ 2.6250]^T$, $l=3$ and $\mu=0.05$. Sampling frequency of 10KHz. is considered for real-time implementation. Six test scenarios are considered in this section. They are:

- Test I and II: Sudden jump of $\pm$10Hz. in frequency.
- Test III and IV: Sudden jump of $\pm 45^{\circ}$ in phase.
- Test V and VI: Sudden jump of $\pm$0.5p.u. in amplitude.

Comparative experimental results are given in Fig. 7. Comparative experimental results demonstrate that the proposed AO-FLL has very food convergence time. In all test cases, the phase estimation error of the proposed technique converged faster and with lower peak phase estimation error with respect to SOGI-FLL. In the case of frequency estimation, the proposed technique performed better than SOGI-FLL in terms of convergence time and peak frequency estimation error for Test I, II, V and VI *i.e.* change in amplitude and frequency. However, in the case of phase change, the proposed technique had slightly higher peak phase estimation error although the convergence time of both techniques are similar. Overall, AO-FLL demonstrated better performance than that of SOGI-FLL. This justifies the effectiveness of the proposed modification.

To analyze the sensitivity of the proposed technique, two further tests have been performed considering the presence of DC bias and harmonics. These tests are:

- Test VII: Sudden jump of DC bias bias from 0 to -0.1p.u.
- Test VIII: Harmonics grid voltage signal comprised of $3^{\text{rd}}, 5^{\text{th}}, 7^{\text{th}}$ and 9^{th}order, each having an amplitude of 0.02p.u.

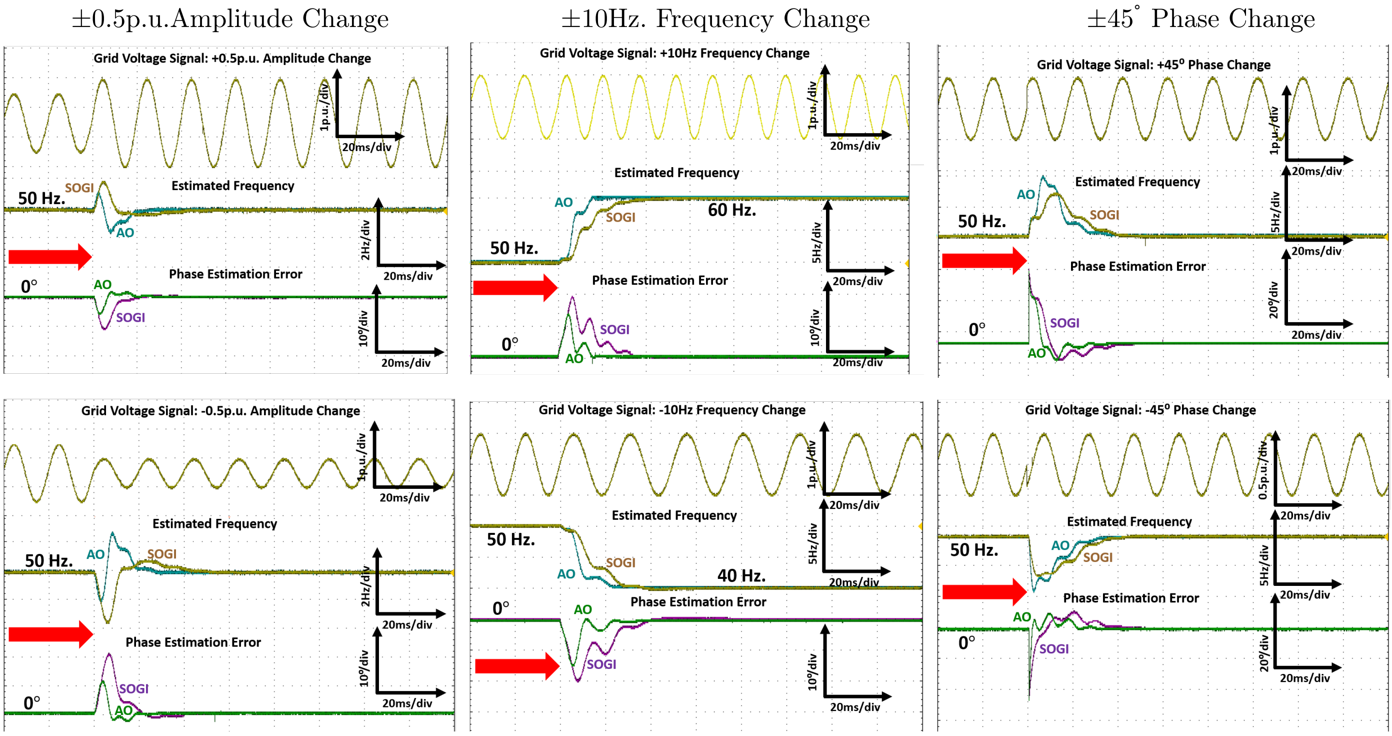

Figure 7: Comparative experimental results for discontinuous jumps in phase, frequency and amplitude.

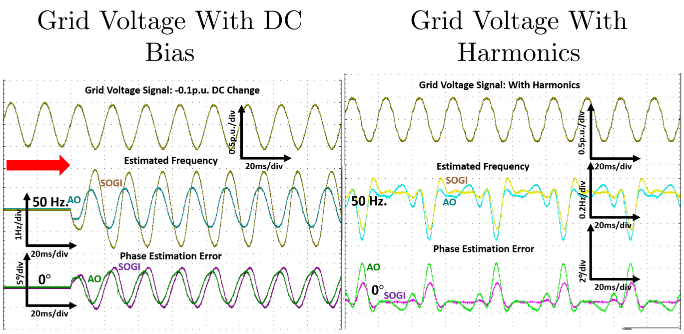

Figure 8: Experimental test results for harmonics and DC bias.

The tests results are given in Fig. 8. Experimental results demonstrate that the proposed technique performs better than SOGI-FLL in terms of DC bias, however, the performance degrades slightly in the presence of harmonics. As a result, one can see that the fast dynamic response came at the cost of reduction in harmonic robustness. To tackle this issue AO-FLL-WPF can be very useful.

All the above tests consider the case with the FLL i.e. we assume that the frequency is unknown. However, one contribution of the current work is to improve the dynamic performance of SOGI-type filter even in the case of fixed frequency. To demonstrate this, let us consider the fixed frequency case i.e. without FLL and $\omega = 2\pi 50$. Suddenly the amplitude jump from 1p.u. to 1.2p.u.In addition, harmonics of 7^{th} and 11^{th} order with amplitude 0.01 p.u. are also suddenly added. Experimental results are given in Fig. 9. From Fig. 9, it can be seen that the proposed observer took slightly more than 0.5 cycle to converge while SOGI took slightly more than 1 cycle to converge. This clearly demonstrates the dynamic performance improvement by the proposed modified SOGI-type adaptive observer even for the fixed frequency case.

4.2. *With pre-filter*

In this Section, the performance of AO-FLL-WPF will be studied in the presence of harmonics. As comparison tools, we have selected SOGI-FLL with pre-loop filter (SOGI-FLL-WPF) [36] and Hybrid Generalized Integrator - FLL (HGI-FLL) [35]. Both of the techniques use pre-loop filter similar to AO-FLL-WPF. The parameters of the techniques are selected as, AO-FLL-WPF: $\nu = 1/\sqrt{2}$ and $L = [1/2\sqrt{2} \quad 1/2\sqrt{2}]^T$, SOGI-FLL-WPF: $k_1 = k_2 = \sqrt{2}$ and $\lambda = 23948$, HGI-FLL : $k_1 = k_2 = \sqrt{2}$ and $\gamma = 15492$. The base signal comprised of 3^{rd}, 5^{th}, 7^{th}, 9^{th}, 11^{th}order harmonics, 20Hz. sub-harmonics and 160Hz.intra-harmonics. All the harmonic components are of 0.1p.u. amplitude. The base signal has 25% total harmonic distortion while the distortions generated by the techniques are given in Fig. 10. Two experimental test scenarios are considered. They are:

- Test-I: +2Hz. change in frequency
- Test-II: −0.5p.u. change in amplitude

Comparative experimental results are given in Fig. 11 and 12. Experimental results demonstrate that although the three techniques have comparable dynamic performance

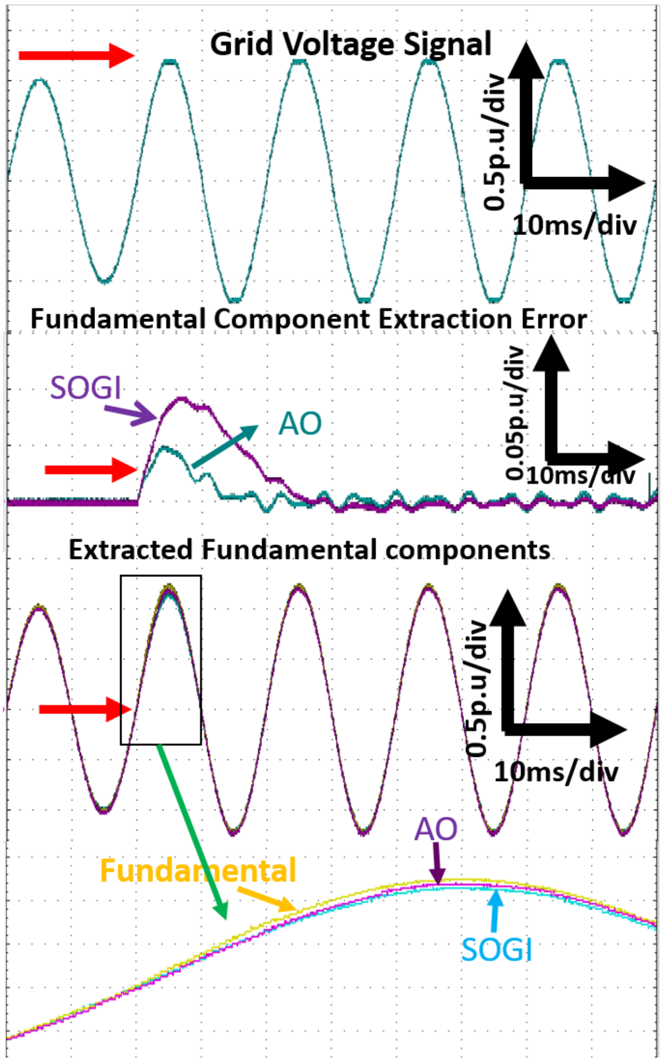

Figure 9: Experimental results for dynamic performance improvement verification test.

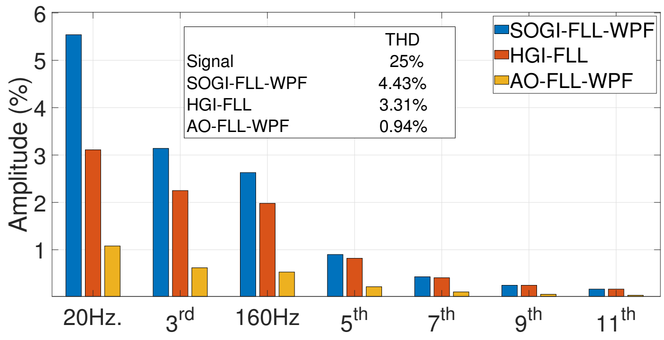

Figure 10: Comparative results of harmonic distortion.

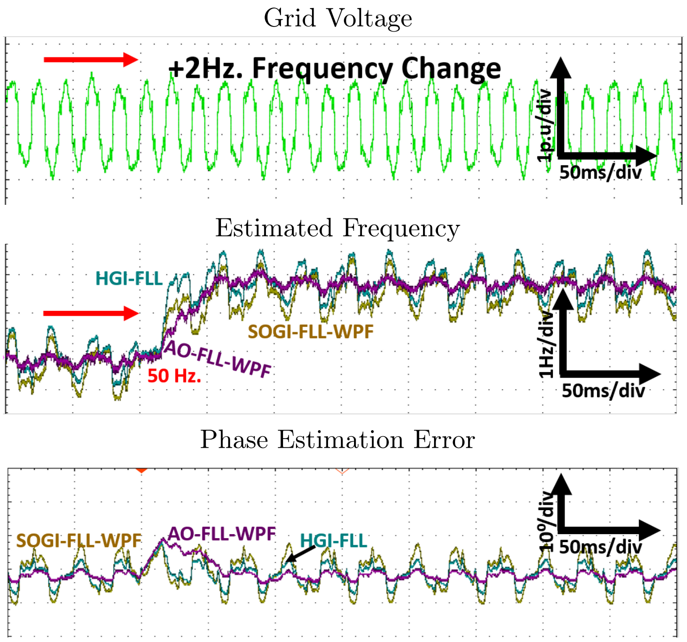

Figure 11: Experimental results for Test-I.

but the proposed AO-FLL-WPF has significantly better steady-state performance. This is evidenced by the steady-state ripple magnitude. Moreover, AO-FLL-WPF had the lowest THD. This is a sign of the proposed technique's good harmonic filtering capability.

4.3. Application to grid synchronization

So far, we have presented our results with synthetic signals, similar to the existing literature. The question that normally arise is how can we use the proposed technique to synchronize any power generators. Let us consider the case of hydro electric power generator as an example. Hydro electric power generator can be connected to the grid in two ways. Firstly by connecting directly the output of the generator to the grid. Secondly, through an inverter. Let us consider the second case. In second case, first the output of the generator is converted to DC through rectifier and the rectified DC voltage is connected to the grid through an inverter. In this type of operation, the generator output is independent of the grid as AC output of the generator is converted to DC. This gives more flexibility to the operation of hydro electric power generator as issue related to the grid doesn't need to be considered in the control of hydro electric generator alone. This essentially means synchronizing the hydroelectric power generator to the grid is the synchronization of the inverter to the grid. To synchronize single-phase inverter to the grid, grid synchronizing current controller (GSCC) is the most popular technique in academic literature and in industrial practice. A grid synchronizing current controller can be seen in Fig. 12 in [39]. To obtain the reference current in GSCC, instantaneous phase, θ of the grid is needed. The proposed technique replaces the PLL in Fig. 12 in [39]. In the presence of harmonics, the proposed technique can reduce the distortion significantly. As result, the estimated phase will be very close to the ideal phase, leading to transferring more power to the grid. It is well known from the literature that maximum power can be transferred only when the output of the inverter and the grid have the same phase.

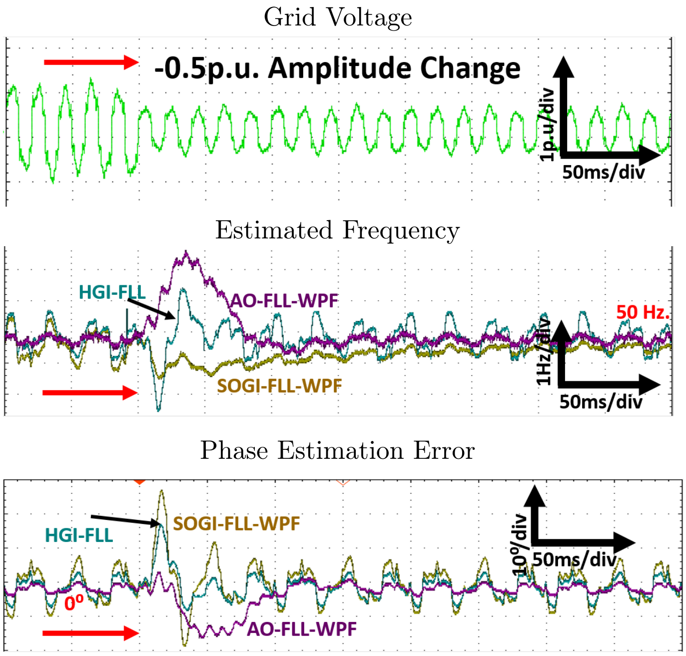

Figure 12: Experimental results for Test-II.

5. Conclusion and Future Works

This paper demonstrated the application of an adaptive observer-based estimation of phase and frequency of single phase grid voltage signal. For this purpose two adaptive observers have been designed. The first one named as AO-FLL, allows arbitrary complex conjugate pole placement. This solves the limited dynamics tuning limits of SOGI-FLL type technique. However, fast dynamic performance is achieved by reducing the robustness to harmonic distortion. To solve this problem, a frequency adaptive pre-loop filtering stage is added to the adaptive observer resulting in a hybrid estimator. Small-signal modeling of the two observers are performed and gain tuning are provided. Comparative experimental results showed the suitability of the proposed observers. It has been observed that AO-FLL-WPF can significantly reduce the harmonic distortion. As we have proposed, two observers, a guideline is need to select select the right observer for practicing engineers. If harmonic robustness is not an issue and fast dynamic response is a priority, then the first observer (i.e. without pre-loop filter) can be considered as a good choice. If the user is interested in harmonic robustness as well as fast dynamic response, then the pre-loop filtered version of the proposed observer can be a good choice. It is to be mentioned here that the proposed solution give much more design freedom than that of SOGI-FLL. Moreover, SOGI-FLL can always be recovered if we set the observer gains as equal. In that regard, the proposed technique adds flexibility in design choice to SOGI-type technique.

The proposed algorithms are nonlinear. However, only linearization-based stability analysis are presented. This guarantees the stability near the equilibrium point. Formal analysis of the operating limit of the proposed algorithm can be considered as a future work. Further improvement of the proposed observers will be considered in a future work. Moreover, the application of the proposed technique to an inverter that is connected to low-inertia distribution grid will also be considered in future works.

References

[1] B. P. McGrath, D. G. Holmes, and J. J. H. Galloway, "Power converter line synchronization using a discrete fourier transform (DFT) based on a variable sample rate," *IEEE Transactions on Power Electronics*, vol. 20, no. 4, pp. 877–884, 2005.

[2] F. D. Freijedo, A. Vidal, A. G. Yepes, P. Fernandez-Comesaña, J. Malvar, O. Lopez, A. Nogueiras, and J. Doval-Gandoy, "WLSE for fast, accurate and robust generation of references in power converter applications," in *Industrial Electronics (ISIE), 2010 IEEE International Symposium on.* IEEE, 2010, pp. 2946–2951.

[3] M. Bettayeb and U. Qidwai, "A hybrid least squares-GA-based algorithm for harmonic estimation," *IEEE transactions on power delivery*, vol. 18, no. 2, pp. 377–382, 2003.

[4] A. Vidal, F. D. Freijedo, A. G. Yepes, P. Fernandez-Comesaña, J. Malvar, O. Lopez, and J. Doval-Gandoy, "A fast, accurate and robust algorithm to detect fundamental and harmonic sequences," in *2010 IEEE Energy Conversion Congress and Exposition.* IEEE, 2010, pp. 1047–1052.

[5] A. Safa, E. M. Berkouk, Y. Messlem, Z. Chedjara, and A. Gouichiche, "A pseudo open loop synchronization technique for heavily distorted grid voltage," *Electric Power Systems Research*, vol. 158, pp. 136–146, 2018.

[6] Z. Oubrahim, V. Choqueuse, Y. Amirat, and M. E. H. Benbouzid, "Maximum-likelihood frequency and phasor estimations for electric power grid monitoring," *IEEE Transactions on Industrial Informatics*, vol. 14, no. 1, pp. 167–177, 2018.

[7] ——, "Disturbances classification based on a model order selection method for power quality monitoring," *IEEE Transactions on Industrial Electronics*, vol. 64, no. 12, pp. 9421–9432, 2017.

[8] V. Choqueuse, A. Belouchrani, F. Auger, and M. Benbouzid, "Frequency and phasor estimations in three-phase systems: Maximum likelihood algorithms and theoretical performance," *IEEE Transactions on Smart Grid*, vol. 10, no. 3, pp. 3248–3258, 2018.

[9] R. Cardoso, R. F. De Camargo, H. Pinheiro, and H. Grundling, "Kalman filter based synchronisation methods," *IET generation, transmission & distribution*, vol. 2, no. 4, pp. 542–555, 2008.

[10] M. Qasim, P. Kanjiya, and V. Khadkikar, "Artificial-neural-network-based phase-locking scheme for active power filters," *IEEE Transactions on Industrial Electronics*, vol. 61, no. 8, pp. 3857–3866, 2014.

[11] L. H. Silva, A. J. Sguarezi Filho, D. A. Fernandes, F. F. Costa, and A. J. M. Cardoso, "A robust phase-locked loop against fundamental frequency deviations and harmonic distortions," *Electric Power Systems Research*, vol. 163, pp. 338–347, 2018.

[12] A. Kulkarni and V. John, "Design of a fast response time single-phase PLL with DC offset rejection capability," *Electric Power Systems Research*, vol. 145, pp. 35–43, 2017.

[13] S. Golestan, M. Monfared, F. D. Freijedo, and J. M. Guerrero, "Dynamics assessment of advanced single-phase PLL structures," *IEEE Transactions on Industrial Electronics*, vol. 60, no. 6, pp. 2167–2177, 2013.

[14] H. A. Hamed, A. F. Abdou, E. H. Bayoumi, and E. El-Kholy, "A fast recovery technique for grid-connected converters after short dips using a hybrid structure PLL," *IEEE Transactions on Industrial Electronics*, vol. 65, no. 4, pp. 3056–3068, 2018.

[15] M. E. Meral and D. Çelik, "Benchmarking simulation and theory of various PLLs produce orthogonal signals under abnormal

electric grid conditions," *Electrical Engineering*, vol. 100, no. 3, pp. 1805–1817, 2018.

[16] H. A. Hamed, A. F. Abdou, E. H. Bayoumi, and E. El-Kholy, "Frequency adaptive CDSC-PLL using axis drift control under adverse grid condition," *IEEE Transactions on Industrial Electronics*, vol. 64, no. 4, pp. 2671–2682, 2017.

[17] C. H. da Silva, R. R. Pereira, L. E. B. da Silva, G. Lambert-Torres, B. K. Bose, and S. U. Ahn, "A digital PLL scheme for three-phase system using modified synchronous reference frame," *IEEE Transactions on Industrial Electronics*, vol. 57, no. 11, pp. 3814–3821, 2010.

[18] T. A. Youssef and O. Mohammed, "Adaptive SRF-PLL with reconfigurable controller for microgrid in grid-connected and stand-alone modes," in *2013 IEEE Power & Energy Society General Meeting*. IEEE, 2013, pp. 1–5.

[19] H. Ahmed, M. H. Bierhoff, and M. Benbouzid, "Multiple nonlinear harmonic oscillator-based frequency estimation for distorted grid voltage," *IEEE Transactions on Instrumentation and Measurement*, pp. 1–9, 2019.

[20] U. Bose, S. K. Chattopadhyay, C. Chakraborty, and B. Pal, "A novel method of frequency regulation in microgrid," *IEEE Transactions on Industry Applications*, vol. 55, no. 1, pp. 111–121, 2019.

[21] C. Subramanian and R. Kanagaraj, "Rapid tracking of grid variables using prefiltered synchronous reference frame PLL," *IEEE Transactions on Instrumentation and Measurement*, vol. 64, no. 7, pp. 1826–1836, 2015.

[22] N. Jaalam, N. Rahim, A. Bakar, C. Tan, and A. M. Haidar, "A comprehensive review of synchronization methods for grid-connected converters of renewable energy source," *Renewable and Sustainable Energy Reviews*, vol. 59, pp. 1471–1481, 2016.

[23] F. D. Freijedo, A. G. Yepes, O. Lopez, A. Vidal, and J. Doval-Gandoy, "Three-phase PLLs with fast postfault retracking and steady-state rejection of voltage unbalance and harmonics by means of lead compensation," *IEEE Transactions on Power Electronics*, vol. 26, no. 1, pp. 85–97, 2011.

[24] F. D. Freijedo, J. Doval-Gandoy, O. Lopez, and E. Acha, "Tuning of phase-locked loops for power converters under distorted utility conditions," *IEEE Transactions on Industry Applications*, vol. 45, no. 6, pp. 2039–2047, 2009.

[25] H. Ahmed, S. Amamra, and I. Salgado, "Fast estimation of phase and frequency for single-phase grid signal," *IEEE Transactions on Industrial Electronics*, vol. 66, no. 8, pp. 6408–6411, Aug 2019.

[26] A. Kherbachi, A. Chouder, A. Bendib, K. Kara, and S. Barkat, "Enhanced structure of second-order generalized integrator frequency-locked loop suitable for DC-offset rejection in single-phase systems," *Electric Power Systems Research*, vol. 170, pp. 348–357, 2019.

[27] P. Rodríguez, A. Luna, I. Candela, R. Mujal, R. Teodorescu, and F. Blaabjerg, "Multiresonant frequency-locked loop for grid synchronization of power converters under distorted grid conditions," *IEEE Transactions on Industrial Electronics*, vol. 58, no. 1, pp. 127–138, 2011.

[28] M. Karimi-Ghartemani, "Linear and pseudolinear enhanced phased-locked loop (EPLL) structures," *IEEE transactions on industrial electronics*, vol. 61, no. 3, pp. 1464–1474, 2014.

[29] H. Ahmed, S. Amamra, and M. H. Bierhoff, "Frequency-locked loop based estimation of single-phase grid voltage parameters," *IEEE Transactions on Industrial Electronics*, vol. 66, no. 8856-8859, pp. 8856–8859, 2019.

[30] M. L. Pay and H. Ahmed, "Modeling and tuning of circular limit cycle oscillator FLL with pre-loop filter," *IEEE Transactions on Industrial Electronics*, 2019.

[31] S. Biricik, H. Komurcugil, N. D. Tuyen, and M. Basu, "Protection of sensitive loads using sliding mode controlled three-phase DVR with adaptive notch filter," *IEEE Transactions on Industrial Electronics*, vol. 66, no. 7, pp. 5465–5475, 2019.

[32] R. S. R. Chilipi, N. Al Sayari, K. H. Al Hosani, and A. R. Beig, "Adaptive notch filter-based multipurpose control scheme for grid-interfaced three-phase four-wire dg inverter," *IEEE Transactions on Industry Applications*, vol. 53, no. 4, pp. 4015–4027, 2017.

[33] X. Quan, X. Dou, Z. Wu, M. Hu, and F. Chen, "A concise discrete adaptive filter for frequency estimation under distorted three-phase voltage," *IEEE Transactions on Power Electronics*, vol. 32, no. 12, pp. 9400–9412, 2017.

[34] C. M. Hackl and M. Landerer, "Modified second-order generalized integrators with modified frequency locked loop for fast harmonics estimation of distorted single-phase signals," *arXiv preprint arXiv:1902.04653*, 2019.

[35] F. Chishti, S. Murshid, and B. Singh, "Weak grid intertie WEGS with hybrid generalized integrator for power quality improvement," *IEEE Transactions on Industrial Electronics*, 2019.

[36] S. Golestan, J. M. G. GE, J. Vasquez, A. M. Abusorrah, and Y. A. Al-Turki, "Modeling, tuning, and performance comparison of advanced second-order generalized integrator-based FLLs," *IEEE Transactions on Power Electronics*, vol. 33, no. 12, pp. 10 229 – 10 239, 2018.

[37] J. Matas, M. Castilla, J. Miret, L. G. de Vicuña, and R. Guzman, "An adaptive prefiltering method to improve the speed/accuracy tradeoff of voltage sequence detection methods under adverse grid conditions." *IEEE Trans. Industrial Electronics*, vol. 61, no. 5, pp. 2139–2151, 2014.

[38] S. H. Strogatz, *Nonlinear dynamics and chaos: with applications to physics, biology, chemistry, and engineering.* CRC Press, 2018.

[39] A. Micallef, "Review of the current challenges and methods to mitigate power quality issues in single-phase microgrids," *IET Generation, Transmission & Distribution*, vol. 13, no. 11, pp. 2044–2054, 2018.